Supplementary Material

S1. Direct measurements of suspended sediment concentration and vertical accretion

We measured SSC and vertical accretion at seven tidal marsh sites spanning the eastern coast of the US and one on the eastern coast of Australia. Four of these sites were located at approximately mean tide level (between -0.05 and 0.06 half-tide units, where 0.0 is mean tide level and 1.0 is MHHW) in youthful marshes at Plum Island Ecosystems Long Term Ecological Research station (PIE LTER; Coleman and Kirwan, 2020), Virginia Coastal Reserve LTER (VCR LTER; Coleman and Kirwan 2018), Chesapeake Bay National Estuarine Research Reserve (CB NERR; Coleman and Kirwan 2021b), and Georgia Coastal Ecosystems LTER (GCE LTER; Coleman and Kirwan 2021a), respectively (Figure 1). The three additional sites were at secondary locations in the PIE LTER and the GCE LTER and a site in Australia. We conducted long term turbidity measurements on the marsh platform, site-specific SSC calibrations, and direct accretion measurements at these four low marsh sites. The three additional sites were monitored for shorter durations (maximum=2 months) and either relied on measurements from other studies or were at higher elevations. All monitored sites were included within the meta-analysis.

Optical backscatter turbidity probes were deployed on the marsh platform and in the adjacent tidal creek to determine the channel SSC and average SSC for the marsh. Our basic approach to measuring SSC follows methods described in previous work at the GCE LTER and PIE LTER (Coleman and Kirwan, 2019; Coleman et al., 2020), where 3-6 sensors were deployed across a transect from tidal channel to marsh interior, measuring

turbidity every 15 minutes for the length of the deployment (1-15 months). Pressure transducers were used to calculate water depth, which was used to estimate tidal range and to remove data points corresponding to time periods when the marsh was not flooded. Turbidity was converted to SSC via *in situ* field calibrations and lab calibrations with native sediment from each site (Coleman and Kirwan, 2019). All calibration equations are in the form of SSC=Turbidity*Calibration Coefficient. The calibration coefficients for the PIE LTER, VCR LTER, CB NERR, and GCE LTER are 2.26 (R^2=0.98), 1.31 (R^2=0.99), 1.04 (R^2=0.98), and 1.33 (R^2=0.93), respectively. Suspect data points were removed from the SSC time series following Ganju et al. (2005). These points represent times when the sensor may have been obstructed by vegetation, or subject to fouling. The SSC time series demonstrate distinct tidal patterns and changes in concentration with distance into the marsh (see Coleman and Kirwan, 2019; Coleman et al., 2020; Supplementary Figure 2). Nevertheless, here we define the SSC of each site simply as the average over-marsh concentration calculated from the entire record of all marsh sensors at a given site.

We measured short-term accretion using sediment tiles made of 14.5 cm x 14.5 cm plastic grids with 1.5 cm^2 openings cut from fluorescent tube lighting covers installed flush to the marsh surface (Coleman et al., 2019). These grids allow plants to grow through them and represent a natural surface for sediment accumulation. On subsequent visits to the sites, we measured the thickness of sediment that had accumulated on the grid to calculate an accretion rate. Sediment tile deployments varied in length, from 9-24 months.

Long-term accretion rates were calculated from the vertical distribution of excess Pb-210 ($^{210}Pb_{xs}$) in sediment cores (15 cm diameter x 100 cm length) collected from each study sites. Each core was sectioned at 1-cm interval with a subset of intervals (every other sample for top 20 cm and every fourth sample beyond 20 cm) prepared for radiometric analysis. Briefly, each interval was dried, pulverized, quantitatively spiked with 6.0 dpm (100 mBq) of polonium-209 (^{209}Po), and reacted with hot (nitric and hydrochloric) acids to leach ^{210}Po (granddaughter of ^{210}Pb) from sediments. Leachate was conditioned following a modified procedure of Flynn (1968) (also reviewed by Sethy et al. 2015) to promote the spontaneous deposition of Po-isotopes on silver (Ag) planchets. The planchets were measured on alpha spectrometry to quantify both ^{209}Po (4.86 MeV) and ^{210}Po (5.41 MeV) isotopes. Leachable ^{210}Po (and ^{210}Pb) was quantified by multiplying the ^{209}Po activity-to-count rate-ratio by the ^{210}Po count rate. Excess ^{210}Pb was assumed to be in secular equilibrium and thus equivalent to acid-leached polonium-210 (^{210}Po). Average accretion rates were estimated using log-linear relationships between $^{210}Pb_{xs}$ and depth in the core following Robbins and Edgington (1975). Mid-depth samples (four to five samples between approximately 15 and 45 cm in select cores) were also analyzed for cesium-137 (^{137}Cs) to supplement $^{210}Pb_{xs}$-based accretion rates, when the latter results were inconclusive. Dry and pulverized samples were sealed in a container and measured on a Canberra (now Mirion Technologies, Inc.) Low-Energy, Germanium (LeGe) detector using the 661.7 keV photopeak. Self-absorption correction for samples followed Cutshall et al. (1983).

The four low marsh monitored sites (Supplementary Table 2) ranged in over-marsh SSC from approximately 5-30 mg L^{-1}, TR from 1.1-3.6 m, and accretion rate from

approximately 7-27 mm yr^{-1}. Spatially, SSC was highest in the tidal channel at all sites, except for the CB NERR site which has a sandy berm proximal to the marsh interior sensor. Temporally, SSC tended to be the highest at mid-tide, presumably coincident with the fastest flow velocities. For the low marsh portions of the sites, the PIE LTER and the CB NERR had the lowest SSC (5.2 and 13.4 mg L^{-1}, respectively) and lower accretion rates, which were successfully determined with ^{210}Pb (6.6 and 7.3 mm yr^{-1}, respectively; Supplementary Figure 3). SSC was higher at the VCR LTER (27.7 mg L^{-1}) and GCE LTER (31 mg L^{-1}), but accretion rates could not be determined with ^{210}Pb because the sites were accreting too rapidly or experienced erosion. Similarly, ^{137}Cs results were inconclusive as concentrations were either too low to measure (VCR LTER) or did not change with depth (GCE LTER). Instead, we calculated accretion rates at these sites from sediment grids (27 and 24 mm yr^{-1}, respectively; Supplementary Figure 4). These short-term accretion rates were verified by comparing them to other studies in the system and estimates of accretion based on the timing of vegetation colonization in aerial photographs and changes in organic content, bulk density, and water content observed in sediment cores. The accretion rate of all four sites (long-term rates for the PIE LTER and CB NERR and short-term rates for the VCR LTER and GCE LTER) were greater than the local relative SLR rate and similar to numerical model-predicted threshold SLR rates (Schuerch et al. 2018; Figure 3a).

S2. Meta-analysis and Empirical Model Formulation

Data from the literature were compiled to include a wider range of salinities, vegetation types, elevations, SSC, TR, and accretion. We included data from an

additional 70 tidal marshes (for a total of 77 sites) where there were direct measurements of SSC and accretion from around the world (Supplementary Table 1). The greatest concentration of sites was in Europe (25 sites) and North America (47 sites). The sites had a range of SSC of 0.5-358 mg L^{-1}, TR of 0.3-12 m, and accretion rates of 1-400 mm yr^{-1}. In situations where SSC and accretion data came from different sources, sites were only included if measurements were conducted within 2 km and 15 years from one another.

We removed outliers from the significant linear relationship between SSC*TR and accretion (eq. 1) to determine the empirical model coefficient most useful for fitting the data to a linear trend. First, all points were used for creating a linear model between SSC*TR and accretion; then, we identified the data point with the largest residual error and calculated a new linear model excluding this data point. Data points were removed in sequence until the removal of an additional outlier had a negligible effect on the slope of the relationship between SSC*TR and accretion based on an analysis of the derivative of the change in slope with the number of outliers removed. Removing 5 of the 77 marsh sites was deemed most appropriate. This approach removes variability from the linear regression so that the resulting slope (C_1) is representative of the majority of the data but not overly influenced by extreme data points.

We analyzed several potential equations to determine the best empirical relationship between SSC, TR, and vertical accretion (Supplementary Table 3). The simplest empirical equation is analogous to a fixed proportion of the sediment suspended in the flooding waters being converted to vertical marsh accretion (equation 1), and therefore does not include *in situ* organic accretion. We then binned marsh sites into 6

groups based on spring tidal range. A plot of the slope of linear regressions between measured accretion and SSC*TR for each tidal range group appeared as a logistic curve, which was then used to define a second model (Supplementary Table 3). For a third empirical model, we determined the best fit linear model (Supplementary Table 3). The simplistic equation predicted accretion as well as the two more complex equations (Supplementary Table 3).

S3. Influence of Different Methodology

Accretion rates and SSC measurements vary with timescale and location of sampling (Christiansen et al., 2000; Parkinson et al. 2016; Breithaupt et al., 2018; Coleman et al., 2020) so we analyzed the relationship between SSC and vertical accretion separately for different methods of measuring accretion and SSC. Accretion methods were classified as radiochronology (Pb210, Cs137), modern sediment deposition (sediment tiles and marker horizons), or modern elevation change (surface elevation tables). We distinguished between measurements of SSC made with bottle sampling and automated sensors, and between measurements made in the channel and over the flooded marsh. For each methodological approach, we calculated the slope between measured accretion and SSC*TR (C_1 in equation 1).

The slope calculated using modern accretion rates was slightly greater but not significantly different than the slope calculated using elevation change rates (modern accretion C_1=0.2452 ± 0.009; elevation change C_1=0.1980 ± 0.019; Figure 2b). The main difference between these approaches is that shallow subsidence is incorporated into elevation change measurements but not accretion measurements (Cahoon et al., 1995;

Cahoon et al. 2006; Jankowski et al. 2017). Our results therefore suggest that shallow subsidence is not a significant contributor to short-term elevation change for a given TR and SSC at the spatial scales and levels of observational uncertainty considered in our study. The slope calculated using only radiochronological measurements was significantly lower than that derived from other approaches (C_1=0.1014 ± 0.008), indicating that accretion rates measured over long timescales are lower than rates measured over short timescales for a given SSC and TR. Our work therefore adds to the growing body of literature identifying a "timescale bias" in which apparent accretion rates decrease with increasing timescale (Breithaupt et al., 2018). Lower apparent accretion rates could be explained by accretion rates that decline as youthful marshes approach an equilibrium elevation (Redfield, 1972), a longer period of time for compaction and organic matter decomposition (Bartholdy et al., 2010), and/or accretion rates averaged over periods of time with slower SLR (Kirwan et al., 2016). The impacts of shallow subsidence are likely being masked by the variability in accretion rates between sites, whereas the impact of long-term subsidence may be too large to be masked by inter-marsh variability. In any case, our finding that accretion rates are significantly lower when measured over longer timescales is consistent with previous work that highlights the influence of long-term subsurface elevation loss in long-term accretion rates (Kearney et al., 1994; Bartholdy et al., 2010; Tornqvist et al., 2008; Horton et al. 2018; Tornqvist et al. 2020; Saintilan et al. 2020), as well as the observation that accretion rates have increased in response to the recent acceleration in the rate of SLR (Kolker et al., 2010; Hill and Anisfeld 2015). Short-term accretion rates potentially underestimate marsh vulnerability because they do not fully account for subsurface

processes that manifest over longer time periods (Parkinson et al., 2017), whereas long-term accretion rates overestimate marsh vulnerability because accretion rates increase in response to accelerating rates of SLR (Kirwan et al., 2017). Since the best approach for assessing wetland vulnerability is unclear (Breithaupt et al., 2018), we incorporate both long-term and short-term measurements of accretion in our empirical modeling (Figures 2 and 3). This approach allows us to quantify the impact of different methods over a broad range of environmental conditions and shows that methodological differences increase with greater sediment availability and more rapid rates of accretion (Figure 2b).

We also explored how the relationship between accretion and SSC*TR depends on differences in the SSC measurement methodology. Sites were grouped based on whether SSC was measured via bottle sampling or automated sensors, and whether SSC measurements were made in the channel or over the flooded marsh. Although the different SSC measurement approaches had different values of C_1, it is difficult to determine how generalizable the results are (Supplementary Figure 5). Measurements made by sensors and measurements over the marsh (n=31; n=16) were less common and covered a narrower range of SSC values than measurements made with bottle sampling and in the channel (n=46; n=61). Although previous work suggests strong temporal variability in SSC that may only be captured with sensors or sampling over long durations (Coleman et al., 2020), and strong spatial gradients between SSC measured in channels and SSC across the marsh platform (Christiansen et al., 2000; Leonard and Reed, 2002; Poirier et al., 2017), there was insufficient information to sufficiently understand the effect of SSC methodology on the relationship between accretion and SSC. We consequently combined all SSC measurement methods in our meta-analysis and

empirical modeling, and note that significant trends between accretion and SSC emerge despite this potential variability.

S4. Global Analysis Methodology

The global modelling of sediment balances is based on the Global Coastal Wetland Model by Schuerch et al. (2018). This relies on the global database from the DIVA including TR and areal coastal wetland data (McOwen et al., 2017), attributed to a total of 12,148 coastline segment of varying length (depending on bio-physical and socio-economic coastline characteristics; Spencer et al., 2016). Spring tidal range data were derived from a new global tidal range dataset (Pickering et al. 2017) using the global tide model OTISmpi (Egbert et al., 2004). Mean spring high water levels and mean spring low water levels were retrieved from a 15-day sea-level reconstruction based on the tidal constituents M2, S2, K1 and O1 (Schuerch et al. 2018).

Our initial goal was to use the empirical model to calculate the spatial extent of expected marsh drowning under different SLR rates. However, we found that the GlobColour satellite-derived SSC data used by DIVA database was considerably lower than and inconsistently related to the SSC in our meta-analysis (Supplementary Figure 1). We suggest that this discrepancy is due to the resolution of the satellite data (4.6km; GlobColour, 2020), which presumably includes low-SSC waters further offshore. This suggests limitations in predicting global threshold rates of SLR and that previous estimates of marsh vulnerability (e.g. Schurech et al., 2018) may be conservative. We instead consider the SSC_{crit} needed for marsh accretion, based on DIVA TR and relative

SLR data, and our empirical model coefficients that predict marsh accretion under these physical parameters.

SSC_{crit} for each coastline segment was calculated as a function of spring TR and global sea-level rise for current (3 mm yr^{-1}) and accelerated rates (6 and 10 mm yr^{-1}). Global sea-level rise rates were adjusted by regional vertical land movement due to glacial isostatic adjustment (Peltier et al., 2004) and accelerated land subsidence in delta regions (Nicholls et al., 2021) to derive regional relative sea-level rise (RSLR) rates. The gravitational changes associated with loss of ice mass in Greenland is not included in the calculation of RSLR rates. Overall, this approach highlights that marshes in certain locations, such as major deltas, experience more rapid rates of sea level rise and will therefore require greater accretion rates to maintain elevation and/or survive. Based on equation 1, and assuming that the maximum possible accretion rate equals RSLR, SSCcrit was calculated as follows:

$$SSC_{crit} = RSLR/(C_1 * TR) \quad (3)$$

The resulting SSC_{crit} values were binned into five categories for which total saltmarsh areas were calculated.

To explore the effect of SLR on marsh vulnerability, we calculated the percentage of global marsh area that would require SSC greater than a reference value under different scenarios of accelerated SLR. Like our previous analyses, we consider both the SSC_{crit} needed to maintain marshes at their current elevation, and the SSC_{crit} needed for marshes to survive. “Maintain” refers to the ability of the high marsh to accrete at the rate of SLR and thus remain high marsh. “Survive” refers to the ability of the low marsh to accrete at the rate of SLR and thus avoiding drowning. We use 30 mg L^{-1} as a reference

229 value as the median SSC of our dataset is 33 mg L^{-1} and the average SSC for U.S. coastal
230 rivers is 30.3 mg L^{-1} (Weston 2014). Concentrations of suspended sediment are declining
231 in rivers throughout the world (Wang et al., 2011; Weston 2014), meaning this reference
232 value may not be representative of average SSC in the future. We find that approximately
233 35% of global marsh area requires SSC > 30 mg L^{-1} to maintain elevation under the
234 current rate of eustatic SLR (3 mm yr^{-1}), and that this percentage increases with SLR (i.e.
235 77% at 10 mm yr^{-1}) (Figure 4a). However, to survive current SLR (3 mm yr^{-1}) only 26%
236 of global marsh area requires SSC > 30 mg L^{-1}, increasing to 71% at high rates of SLR
237 (10 mm yr^{-1}) (Figure 4b). This suggests there may be considerable marsh area that can
238 survive current SLR by converting from high marsh to low marsh (i.e. not maintaining
239 elevation). It is important to note that a given ecosystem must be capable of the
240 ecological shifts from high marsh to low marsh for this to remain true. The area capable
241 of surviving SLR but not maintaining the current elevation distribution under SLR
242 decreases at higher SLR rates, where marsh survival requires substantially higher SSC.
243

Supplemental References

Bartholdy, J., J. B. T. Pedersen, and A. T. Bartholdy. 2010. Autocompaction of shallow silty salt marsh clay. Sedimentary Geology 223: 310–319. https://doi.org/10.1016/j.sedgeo.2009.11.016

Cahoon, D. R., D. J. Reed, and J. W. Day Jr. 1995. Estimating shallow subsidence in microtidal salt marshes of the southeastern United States: Kaye and Barghoorn revisited. *Mar. Geol.* 128: 1–9. https://doi.org/10.1016/0025-3227(95)00087-F

Coleman, D. J., and M. L. Kirwan. 2019. The effect of a small vegetation dieback event on salt marsh sediment transport. *Earth Surf. Process. Landf.* 44: 944–952. doi:10.1002/esp.4547

Cutshall, N. H., I. L. Larsen, and C. R. Olsen. 1983. Direct analysis of 210Pb in sediment samples: Self-absorption corrections. *Nucl. Instrum. Methods B* 206: 309–312. https://doi.org/10.1016/0167-5087(83)91273-5

Egbert, G. D., R. D. Ray, and B. G. Bills. 2004. Numerical modeling of the global semidiurnal tide in the present day and in the last glacial maximum. *J. Geophys. Res. Oceans* 109: C03003. https://doi.org/10.1029/2003JC001973

Flynn, W. W. 1968. The determination of low levels of polonium-210 in environmental materials. *Anal. Chim. Acta* 43: 221–227. https://doi.org/10.1016/s0003-2670(00)89210-7

Ganju, N. K., D. H. Schoellhamer, and B. A. Bergamaschi. 2005. Suspended sediment fluxes in a tidal wetland: Measurement, controlling factors, and error analysis. *Estuaries* 28: 812–822. https://doi.org/10.1007/BF02696011

GlobColour (France: ACRI-ST; 2020). Product user's guide. Version 4.2, Reference GC-UM-ACR-PUG-01

Hill, T. D., and S. C. Anisfeld. 2015. Coastal wetland response to sea level rise in Connecticut and New York. *Estuar. Coast. Shelf Sci.* 163: 185–193. https://doi.org/10.1016/j.ecss.2015.06.004

Kearney, M. S., J. C. Stevenson, and L. G. Ward. 1994. Spatial and temporal changes in marsh vertical accretion rates at Monie Bay: Implications for sea-level rise. *J. Coast. Res.*: 10 (4):1010–1020. https://www.jstor.org/stable/4298292

Kirwan, M. L., S. Temmerman, G. R. Guntenspergen, and S. Fagherazzi. 2017. Reply to "Marsh vulnerability to sea-level rise". *Nat. Clim. Change* 7: 756–757. https://doi.org/10.1038/nclimate3425

McOwen, C., and others. 2017. A global map of saltmarshes. *Biodivers. Data J.* 5: e11764. https://dx.doi.org/10.3897%2FBDJ.5.e11764

Peltier, W. 2004. Global glacial isostasy and the surface of the ice-age earth: The ice-5G (VM2) model and GRACE. *Annu. Rev. Earth Planet. Sci.* 32: 111–149. https://doi.org/10.1146/annurev.earth.32.082503.144359

Pickering, M. D., K. J. Horsburgh, J. R. Blundell, J. J. M. Hirschi, R. J. Nicholls, M. Verlaan, and N. C. Wells. 2017. The impact of future sea-level rise on the global tides. *Cont. Shelf Res.* 142: 50–68. https://doi.org/10.1016/j.csr.2017.02.004

Redfield, A. C. 1972. Development of a New England salt marsh. *Ecol. Monogr*. 42: 201–237. https://doi.org/10.2307/1942263

Robbins, J. A., and D. N. Edgington. 1975. Determination of recent sedimentation rates in Lake Michigan using Pb-210 and Cs-137. *Geochim. Cosmochim. Acta* 39: 285–304. https://doi.org/10.1016/0016-7037(75)90198-2

Sethy, N. K., A. K. Sutar, P. Rath, V. N. Jha, P. M. Ravi, and R. M. Tripathi. 2015. A review of radio chemical analysis and estimation of 210Po in soil matrices. *J. Radiat. Res. Appl. Sci.* 8: 590–596. https://doi.org/10.1016/j.jrras.2015.07.001

Törnqvist, T. E., and others. 2008. Mississippi Delta subsidence primarily caused by compaction of Holocene strata. *Nat. Geosci.* 1: 173–176. https://doi.org/10.1038/ngeo129

Supplementary Table S1: List of all sites included in the meta-analysis, including country name or state abbreviation for sites located in the US. Source refers to the original data source. All suspended sediment concentrations (SSC) are in mg L^{-1}, Accretion rates (Acc.) are in mm yr^{-1}, and TR are spring tidal ranges in meters. Marsh or Channel and Sensor or Bottle columns refer to how SSC was measured, with the letter corresponding to the first letter of the methodology. The Acc. Method column refers to how accretion rates were measured and are classified as either radiochronology (R), modern accretion (A), or elevation change (E). If the site was specifically described as a low elevation marsh, it is indicated with an X, and if it was not, then the cell is blank.

Location	*SSC Source*	*SSC*	*Marsh or Channel*	*Sensor or Bottle*	*Accretion Source*	*Acc.*	*Acc. Method*	*Low Marsh*	*TR*
Plum Island, MA	This Study	5.2	M	S	This Study	6.6	R	X	3.6
Upper Plum Island, MA	This Study	4.4	M	S	This Study	11.0	A	X	3.6
Goodwin Island, VA	This Study	13.4	M	S	This Study	7.3	R	X	1.1
Mockhorn Island, VA	This Study	27.6	M	S	This Study	27.0	A	X	1.9
South Altamaha, GA	This Study	31.0	M	S	This Study	24.0	A	X	2.7
North Altamaha, GA	This Study	22.4	C	S	Loomis and Craft 2010	6.6	R		2.7
Currambene Creek, Australia	This Study	0.5	M	S	This Study	1.2	R		1.1
Scheldt Estuary, Netherlands	Temmerman et al. 2004	130	C	B	Temmerman et al. 2004	225	E	X	5.9
Scheldt Estuary, Netherlands	Temmerman et al. 2004	109	C	B	Temmerman et al. 2004	45.5	R	X	5.9
Scheldt Estuary, Netherlands	Temmerman et al. 2004	76	M	B	Temmerman et al. 2004	45.5	R	X	5.9
Scheldt Estuary, Netherlands	Temmerman et al. 2004	41	C	B	Temmerman et al. 2004	29.4	E	X	5.2
Scheldt Estuary, Netherlands	Temmerman et al. 2004	33	C	B	Temmerman et al. 2004	19	R	X	4.8
Scheldt Estuary, Netherlands	Temmerman et al. 2004	29	M	B	Temmerman et al. 2004	19	R	X	4.8
Scheldt Estuary, Netherlands	Temmerman et al. 2004	41	C	B	Temmerman et al. 2004	23.7	E	X	4.8
Scheldt Estuary, Netherlands	Temmerman et al. 2004	61	C	B	Temmerman et al. 2004	35.7	E	X	5.3

Scheldt Estuary, Netherlands	Temmerman et al. 2004	61	C	B	Temmerman et al. 2004	29.3	E	X	5.3
Scheldt Estuary, Netherlands	Temmerman et al. 2004	61	C	B	Temmerman et al. 2004	32.3	E	X	5.3
Scheldt Estuary, Netherlands	Temmerman et al. 2004	104	C	B	Temmerman et al. 2004	23.5	R	X	4.1
Scheldt Estuary, Netherlands	Silinski et al. 2016	62	C	B	Silinski et al. 2016	72	E		5.4
Elbe Estuary, Germany	Kappenberg & Grabeman 2001	120	C	B	Schoutens et al. 2019	150	E	X	3.8
Elbe Estuary, Germany	Kappenberg & Grabeman 2001	120	C	B	Schoutens et al. 2019	80	E	X	3.8
Delaware Bay, DE	Stumpf 1983	5	M	B	Kim et al. 1997	3.5	R		1.8
Cedar Creek, FL	Leonard et al. 1995	12.5	M	B	Leonard et al. 1995	7.2	A		1.2
Choptank River, MD	Ensign et al. 2014	17.5	C	B	Ensign et al. 2014	19	A		1.4
Choptank River, MD	Ensign et al. 2014	21	C	S	Ensign et al. 2014	19	A		1.4
Pocomoke River, MD	Ensign et al. 2014	10	C	B	Ensign et al. 2014	15	A		1
Pocomoke River, MD	Ensign et al. 2014	31	C	B	Ensign et al. 2014	15	A		1
Blackwater Wildlife Refuge, MD	Stevenson et al. 1985	103.5	C	B	Stevenson et al. 1985	3.1	R		0.7
Hengsha Island, Yangzte China	Qing et al. 2003	250	C	B	Yang et al. 2000	276	A	X	4.6
Town Creek, SC	Murphy & Voulgaris 2006	28	C	B	Sharma et al. 1987	2.4	R		2.3
Oyster Landing, SC	Murphy & Voulgaris 2006	30.5	C	B	Sharma et al. 1987	1.4	R		2
Mud Bay, North Inlet, SC	Hutchinson et al. 1995	163.5	C	B	Hutchinson et al. 1995	37	A		1.5
Sixty Bass, North Inlet, SC	Hutchinson et al. 1995	169.1	C	B	Hutchinson et al. 1995	42	A		1.5
Scheld Estuary, Netherlands	Temmerman et al. 2004	130	C	B	Vandenbruwaene et al., 2011	122	E	X	5.9
Scheld Estuary, Netherlands	Wang & Temmerman, 2013	45	C	B	Wang & Temmerman, 2013	25	E	X	4.9
Venice Lagoon, Italy	Venier et al. 2014	20.7	C	S	Bellucci et al. 2007	2.8	R		1.1
Venice Lagoon, Italy	Venier et al. 2014	29.1	C	S	Day et al. 1999	6.5	A		1.1

Venice Lagoon, Italy	Carniello et al. 2012	16.6	C	S	D'Alpaos et al. 2017	7	R	X	1.1
Wadden Sea, Dollart, Germany	Ridderinkhof et al. 2000	100	C	S	Esselink et al. 1998	18	E	X	3.3
Blythe Estuary, England	French et al. 2005	60.9	C	S	French et al. 2005	11.7	E	X	2
Freemans Creek, NC	Ensign & Currin, 2016	20.9	M	B	Currin et al. 2017	10.2	E	X	0.8
Traps Bay Creek, New River, NC	Ensign et al. 2017a	16	C	B	Currin et al. 2017	3.7	E		0.6
French Creek, New River, NC	Ensign et al. 2017a	8	C	B	Currin et al. 2017	3.1	E		0.2
Nelson Island, Plum Island, MA	LeMay 2007	9.3	C	B	Kirwan et al. 2011	2	R		3.6
Club Head Creek, Plum Island, MA	LeMay 2007	11	C	B	Kirwan et al. 2011	2.6	R		3.6
Blackwater Wildlife Refuge, MD	Ganju et al. 2017	63	C	S	Ganju et al. 2015	6	A		0.4
Fishing Bay, MD	Ganju et al. 2017	39	C	S	Ganju et al. 2015	4.7	A		0.8
Ogunquit, ME	Ganju et al. 2017	3.7	C	S	Neil Ganju	3.8	E		2.1
Seal Beach, CA	Ganju et al. 2017	15	C	S	Rosencranz et al. 2017	10	A	X	2.5
Point Mugu, CA	Ganju et al. 2017	15	C	S	Rosencranz et al. 2017	7	A		1.6
Reedy Creek, NJ	Ganju et al. 2017	9.5	C	S	Elsey-Quirk 2016	7	E	X	0.3
Potomac River, VA	Palinkas & Engelhardt 2018	22.1	C	B	Palinkas & Engelhardt 2018	6.9	A		0.9
Bayou Chitigue, LA	Wang 1997	20	C	B	Cahoon et al. 2006	16.8	A	X	0.4
Bayou Chitigue, LA	Day et al. 2011	67	C	B	Day et al. 2011	34.4	A	X	0.4
Old Oyster Bayou, LA	Day et al. 2011	107	C	B	Day et al. 2011	20.6	A	X	0.6
St. Jones, DE	Moskalski & Sommerfield, 2012	6	M	B	Kraft et al. 1992	4.3	R	X	1.7
Bombay Hook, DE	Sommerfield & Wong, 2011	9	C	S	Kraft et al. 1992	6.8	R	X	2.1
Bayou Penchant, LA	Lane et al. 2002	26.2	C	B	DeLaune et al. 1987	7.8	R	X	0.6
Fourleague Bay, LA	Lane et al. 2002	70	C	B	DeLaune et al. 1987	6.5	R	X	0.3
Napa River, CA	Buchanan & Ganju, 2003	49	C	S	Schile et al. 2014	3.2	R		2.9

Mallard Island, CA	Buchanan & Ganju, 2003	41	C	S	Schile et al. 2014	2.7	R		1.7
San Mateo Bridge, CA	Buchanan & Ganju, 2003	37	C	S	Patrick & Delaune, 1990	6	R		3
Far South SF Bay, CA	Buchanan & Ganju, 2003	62	C	S	Watson 2004	28	R		3
Tagus Estuary, Portugal	Vale & Sundby, 1987	32	C	B	Salgueiro & Cacador 2007	37	A	X	4
Skallingen, Denmark	Bartholdy & Anthony 1998	35	C	S	Bartholdy & Madsen 1985	9	R	X	1.6
Sylt, Wadden Sea, Germany	Schuerch et al. 2013	34	M	B	Schuerch et al. 2012	3.5	R		2
Wax Lake Delta, LA	W. Wagner, unpublished	22	C	S	Wagner et al. 2017	14.9	E	X	1
Wax Lake Delta, LA	W. Wagner, unpublished	42	C	S	Wagner et al. 2017	16.9	E	X	1
Dyfi Estuary, Wales	S. Jackson, unpublished	15.7	C	B	Shi 1993	16.0	A		4.5
Delaware Bay Mouth, NJ	Haaf et al. 2019	50	C	B	Haaf et al. 2019	5.7	A		1.5
Delaware River, NJ	Haaf et al. 2019	16	C	B	Haaf et al. 2019	10.0	A		1.9
Barnegut Bay, NJ	Haaf et al. 2019	23	C	B	Haaf et al. 2019	4.2	A		0.4
San Pablo Bay, CA	Lacy et al. 2019	118	M	S	Lacy et al. 2019	8.0	A	X	2.5
Yinshuichuan, Yangtze, China	Chen et al. 2003	358	C	B	Yang et al. 2003	400	A	X	4.3
Suncheon Bay, South Korea	Lee et al. 2008	312	C	B	Lee et al. 2008	55	A	X	3.1
Allen Creek, Canada	Davidson-Arnott et al. 2002	117	M	S	van Proosdij et al., 2006	14	E		12
Kingsport, Canada	Proirier et al. 2017	53	M	S	Proirier et al. 2017	11.4	A		11

305

306 Supplementary Table S2: Additional details on the four low marsh monitoring sites. S. alterniflora form refers to the growth form of *Spartina*
307 *alterniflora*
308

Location	Site Affiliation	S. alterniflora form	Latitude	Longitude	Monitoring Duration	Accretion Verification
Plum Island, MA	PIE LTER	Short	42°43'55.43"N	70°50'30.78"W	9 months	Comparison to Wilson et al. 2014; FitzGerald et al., 2021
Goodwin Island, VA	CB NERR	Tall	37°13'15.35"N	76°24'56.29"W	24 months	Aerial imagery and core properties
Mockhorn Island, VA	VCR LTER	Tall	37°16'51.35"N	75°52'44.83"W	18 months	Aerial imagery and core properties
South Altamaha, GA	GCE LTER	Tall	31°18'10.07"N	81°24'22.52"W	12 months	Aerial imagery and core properties

Supplementary Table S3: The three predictive empirical models used to calculate accretion are given with corresponding constants. The statistical measures are based on a linear regression between measured accretion and accretion predicted using the empirical model. RMSE refers to root mean squared error

Model Type	***Equation***	***Fitted Coefficients***	***RMSE***	***R^2***	***p-value***
1. Simplest	$A = C_1 * SSC * TR$	C_1=0.22	21.3	0.89	<0.001
2. Logistic	$A = \left(\frac{C_1 - C_2}{1 + e^{C_3(TR - C_4)}} + C_2\right) * SSC$	C_1=1.10, C_2=0.18, C_3=-3.45, C_4=3.13	18.7	0.91	<0.001
3. Best Fit Linear	$A = C_1 * SSC + C_2 * TR + C_3 * SSC * TR$	C_1=-0.27, C_2=-10.1, C_3=0.32	18.1	0.92	<0.001

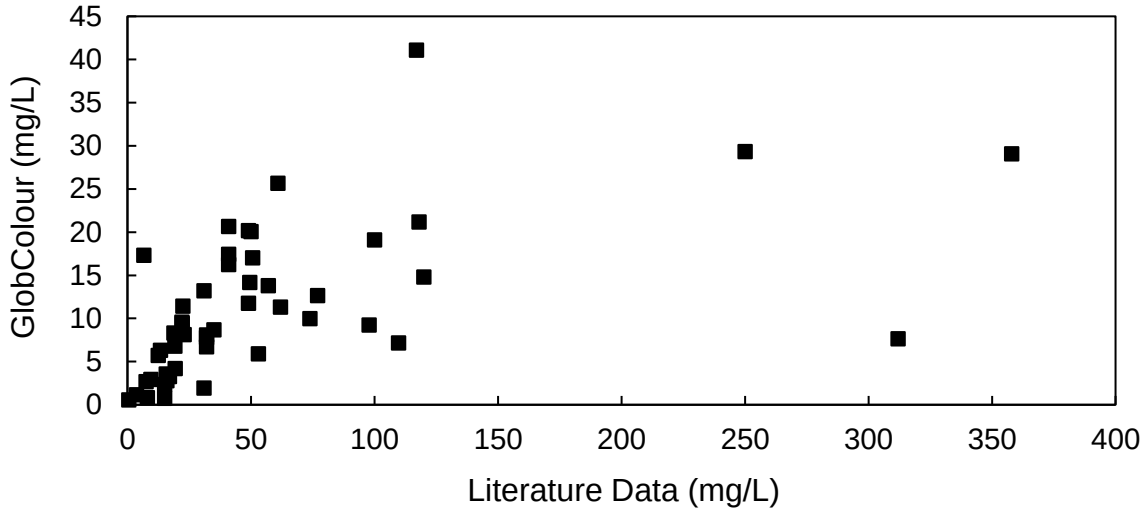

Supplementary Figure S1: Comparison of GlobColour satellite-derived suspended sediment concentrations and literature-derived field measurements (Supplementary Table 1)

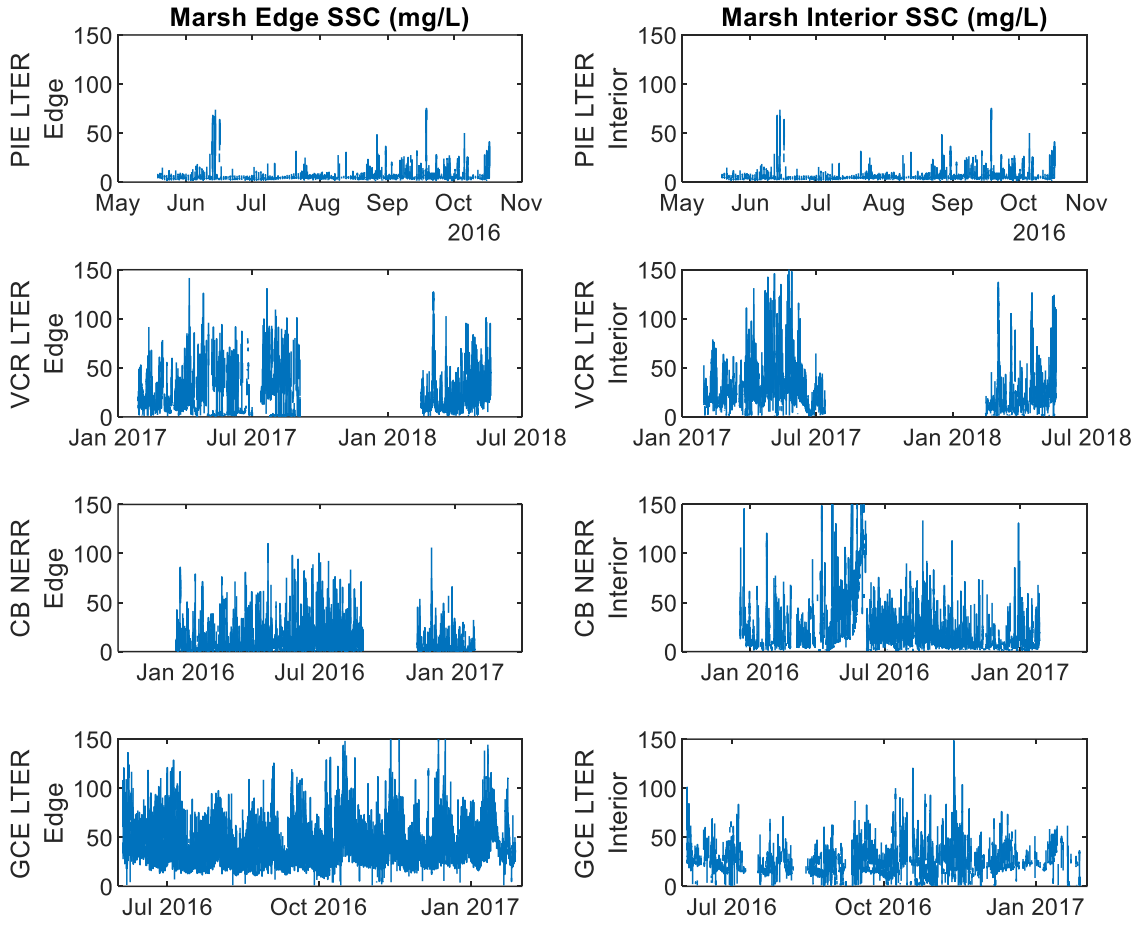

Supplementary Figure S2: Suspended sediment concentration time series of the marsh edge and interior of the four low marsh sites. Note differences in the x-axis that correspond to different monitoring lengths. Gaps in the record represent times when the sensors were being repaired or field conditions prohibited site monitoring.

PIE LTER Edge

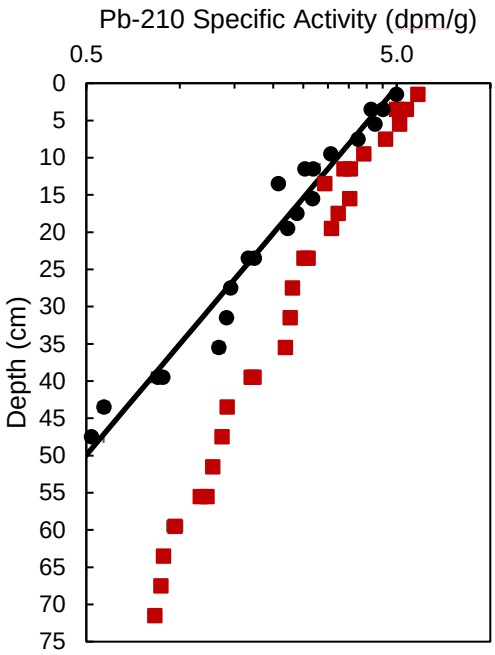

PIE LTER Interior

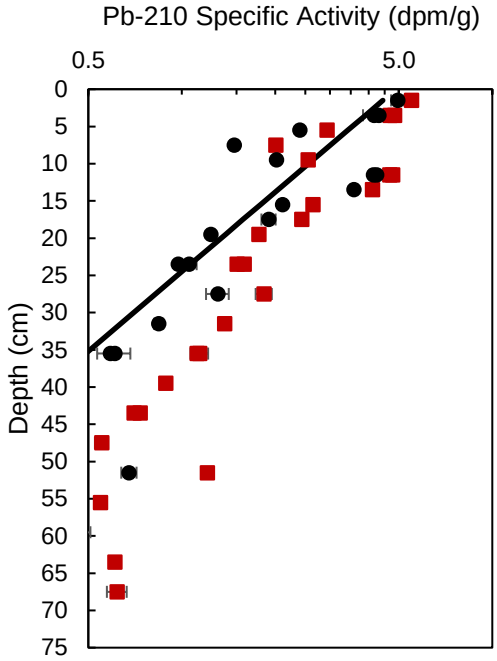

CB NERR Edge

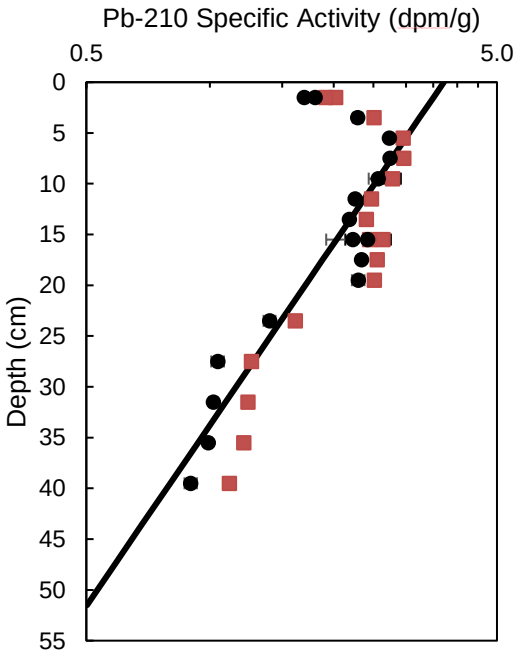

CB NERR Interior

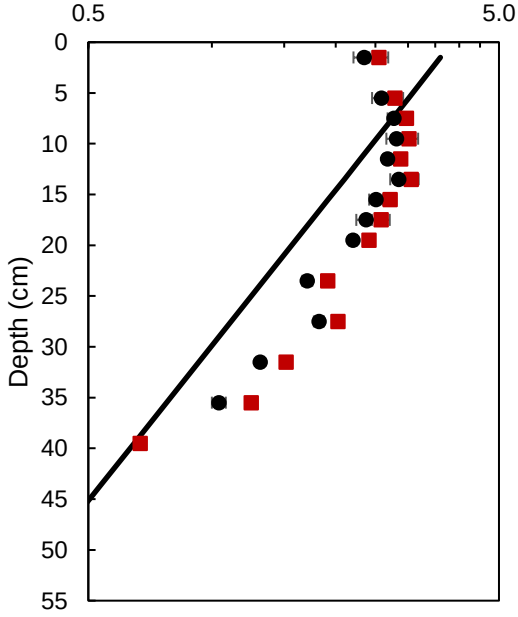

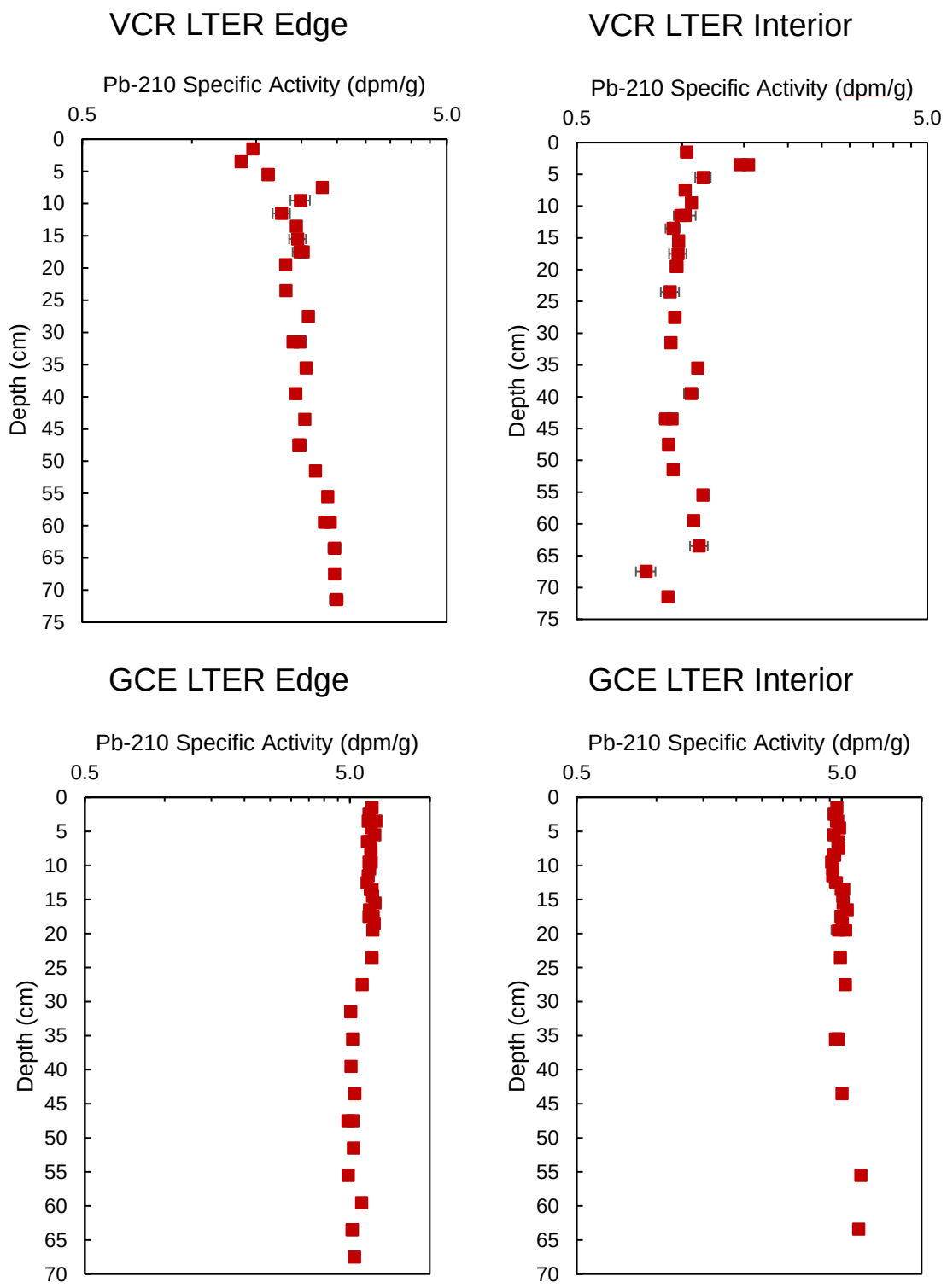

Supplementary Figure S3: Pb-210 total activity (red squares) and excess activity (black circles) in sediment cores from the edge and interior of the four low marsh sites. The PIE LTER interior core was taken from outside of the low marsh, so the edge core accretion rate was used for the site (6.6 mm yr^{-1}). Both CB NERR cores were in the low mash so were averaged to obtain the accretion rate (7.3 mm yr^{-1}). No accretion rate could be calculated for GCE LTER or VCR LTER.

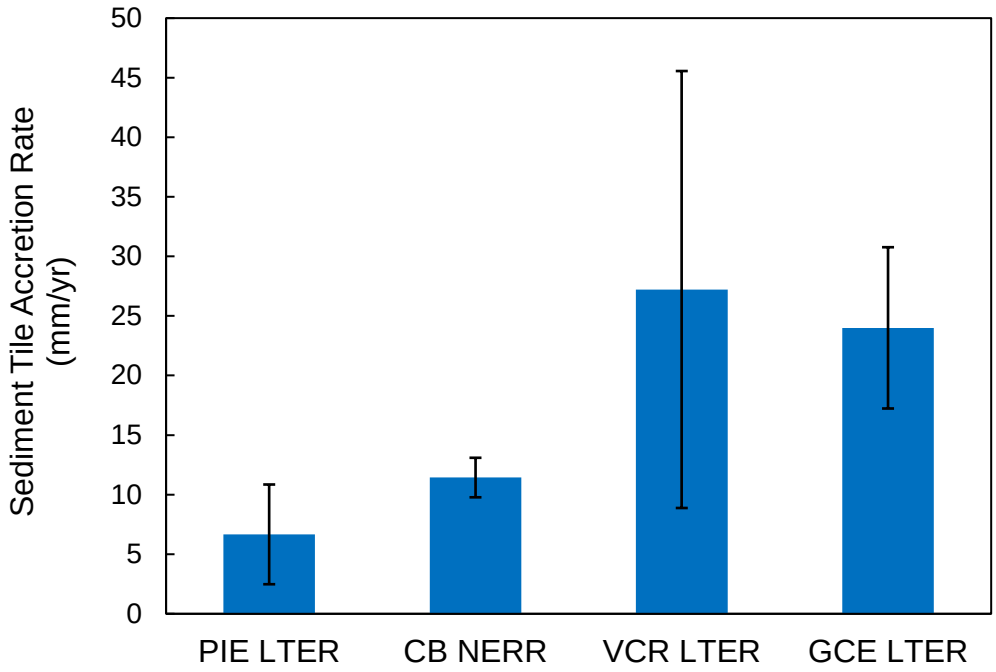

Supplementary Figure S4: Vertical marsh accretion rate measured on top of sediment tiles and/or grids. Error bars represent one standard deviation. The rates shown for the VCR LTER and GCE LTER were used in lieu of radiochronological rates.

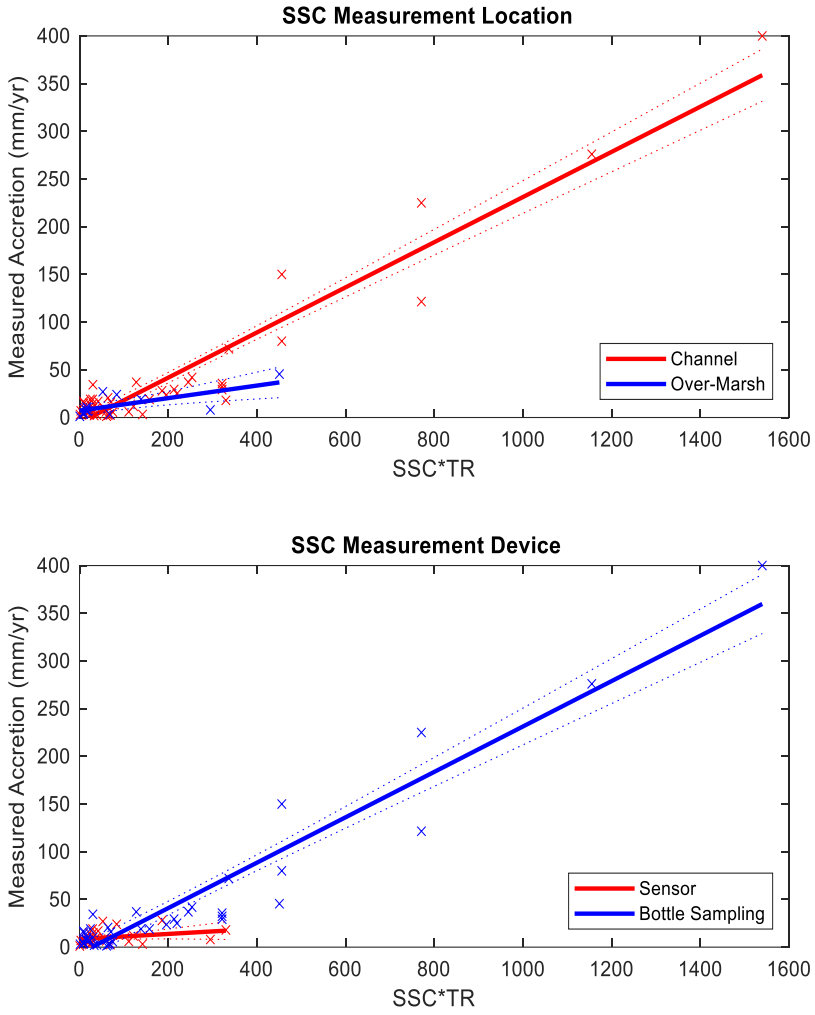

Supplementary Figure S5: Comparison of different suspended sediment concentration measurement methods. Note that channel sampling and bottle sampling are the dominant approaches (62 and 47 sites out of 77, respectively).